J Mater Sci: Mater Med (2006) 17: 437–445
DOI 10.1007/s10856-006-8471-z

In-situ hardening hydroxyapatite-based scaffold for bone repair

Yu Zhang · Hockin H. K. Xu · Shozo Takagi · Laurence C. Chow

Received: 15 July 2004 / Accepted: 7 July 2005

Abstract Musculoskeletal conditions are becoming a major health concern because of an aging population and sports- and traffic-related injuries. While sintered hydroxyapatite implants require machining, calcium phosphate cement (CPC) bone repair material is moldable, self-hardens *in situ*, and has excellent osteoconductivity. In the present work, new approaches for developing strong and macroporous scaffolds of CPC were tested. Relationships were determined between scaffold porosity and strength, elastic modulus and fracture toughness. A biocompatible and biodegradable polymer (chitosan) and a water-soluble porogen (mannitol) were incorporated into CPC: Chitosan to make the material stronger, fast-setting and anti-washout; and mannitol to create macropores. Flexural strength, elastic modulus, and fracture toughness were measured as functions of mannitol mass fraction in CPC from 0% to 75%. After mannitol dissolution in a physiological solution, macropores were formed in CPC in the shapes of the original entrapped mannitol crystals, with diameters of 50 μm to 200 μm for cell infiltration and bone ingrowth. The resulting porosity in CPC ranged from 34.4% to 83.3% volume fraction. At 70.2% porosity, the hydroxyapatite scaffold possessed flexural strength (mean $\pm$ sd; n = 6) of (2.5 $\pm$ 0.2) MPa and elastic modulus of (0.71 $\pm$ 0.10) GPa. These values were within the range for sintered porous hydroxyapatite and cancellous bone. Predictive equations were established by regression power-law fitting to the measured data ($R^2 > 0.98$) that described the relationships between scaffold porosity and strength, elastic modulus and fracture toughness. In conclusion, a new graft composition was developed that could be delivered during surgery in the form of a paste to harden *in situ* in the bone site to form macroporous hydroxyapatite. Compared to conventional CPC without macropores, the increased macroporosity of the new apatite scaffold may help facilitate implant fixation and tissue ingrowth.

H. H. K. Xu (✉) · S. Takagi · L. C. Chow
Paffenbarger Research Center, American Dental Association Foundation.
Tel.: (301) 975-6804
Fax: (301) 963-9143
e-mail: hockin.xu@nist.gov

Y. Zhang
Ceramics Division, National Institute of Standards and Technology, Gaithersburg, MD 20899-8546, USA

1. Introduction

Bone fracture and damage in the United States alone results in more than 1.3 million surgical procedures every year, and this number is predicted to increase dramatically as the life expectancy of the population increases [1, 2]. Hydroxyapatite has found wide use as a bone replacement material due to its chemical and crystallographic similarity to carbonated apatite in human bones and teeth [3–5]. While sintered hydroxyapatite can be machined and used in pre-fabricated forms, calcium phosphate cements can be molded as a paste and hardened *in situ* [6–14]. One promising calcium phosphate cement [6], referred to as CPC, is comprised of a mixture of fine particles of tetracalcium phosphate [TTCP, or $Ca_4(PO_4)_2O$] and dicalcium phosphate anhydrous [DCPA, or $CaHPO_4$]. The CPC powder can be mixed with water to form a paste that can conform to osseous defects with complex shapes, and set *in vivo* to form hydroxyapatite with excellent osteoconductivity [15–21]. One major disadvantage of current orthopaedic implant materials, including sintered hydroxyapatite, is that they exist in a hardened form, requiring the surgeon to fit the surgical site around the implant or to carve the graft to the desired shape. This can lead to increases in bone loss, trauma to the surrounding tissue, and

prolonged surgical time [1]. In this context, CPC's moldability and *in situ* self-hardening ability, together with its excellent osteoconductivity, make it a highly desirable material for orthopaedic repair. CPC is especially promising for use in a number of craniofacial and orthopedic procedures, including the reconstruction of frontal sinus, augmentation of craniofacial skeletal defects, use in endodontics, and the repair of periodontal bone defects [6, 17–21].

In our previous studies, macropores were built into CPC by incorporating particles of mannitol, a water-soluble nontoxic porogen [22, 23]. The set hydroxyapatite was then immersed in a physiological solution to extract the mannitol, thus producing macropores in the shapes of the entrapped crystals [22, 23]. However, only a narrow range of mannitol mass fractions, 0% to 40%, was tested [23]. The effect of mannitol fraction on the fracture toughness of the graft was not investigated, and the porosity-mechanical property relationships were not modeled for the macroporous CPC scaffolds.

In the present study, both mannitol and chitosan lactate, a biocompatible and biodegradable polymer, were incorporated into CPC. The mannitol mass fraction encompassed a wide range from 0% to 75%. The objectives were: (1) to develop a self-hardening hydroxyapatite-based scaffold with mechanical properties matching those of cancellous bone; (2) to determine the scaffold mechanical properties as a function of pore volume fraction; and (3) to establish the porosity-mechanical properties relationships.

2. Materials and methods

2a. Materials

The CPC powder consisted of an equimolar mixture of tetracalcium phosphate (TTCP) powder and dicalcium phosphate anhydrous (DCPA) powder [6, 17–21]. Mannitol ($CH_2OH[CHOH]_4CH_2OH$, Sigma Chemical, St. Louis, MO) was recrystallized in an ethanol/water solution at 50/50 by volume, and then filtered, dried, ground, and sieved through openings of 500 μm (top sieve) and 300 μm (bottom sieve) [22, 23]. Mannitol was selected because it has the appropriate solubility, is non-toxic, and is physiologically compatible [22, 23]. The mannitol powder thus obtained was combined with the CPC powder to form seven mixtures, at mannitol/(mannitol + CPC powder) mass fractions of 0%, 5%, 15%, 30%, 45%, 60%, and 75%.

Chitosan was incorporated into CPC because it is known to be a biocompatible and biodegradable polymer [24–26] and was shown to impart high strength and toughness to non-macroporous CPC in previous studies [27, 28]. Chitosan lactate (referred to as chitosan in this paper; technical grade, VANSON, Redmond, WA) was mixed with distilled water at a mass fraction of 15% to form the CPC liquid. A previous study [29] showed that this mass fraction produced specimens with relatively high strength. This cement liquid was then mixed with each of the seven CPC-mannitol powders to make cement specimens.

A CPC powder:liquid mass ratio of 3.5 was used because preliminary studies showed that this ratio yielded specimens with the highest strength. The CPC-mannitol-chitosan paste was manually mixed using a spatula and placed into stainless steel molds of 3 mm × 4 mm × 25 mm to make flexural specimens. The paste in each mold was sandwiched between two glass slides, and set in a humidor at 100% relative humidity at 37 °C for 4 h. The hardened specimens were demolded and immersed in a simulated physiological solution (1.15 mmol/L Ca, 1.2 mmol/L P, 133 mmol/L NaCl, 50 mmol/L HEPES, buffered to a pH of 7.4) and stored in an oven for 20 h at 37 °C prior to mechanical testing. This immersion dissolved the mannitol and created macropores in the CPC [22, 23].

2b. Mechanical testing

A three-point flexural test with a span of 20 mm was used to fracture the specimens at a crosshead speed of 1 mm/min on a computer-controlled Universal Testing Machine (model 5500R, Instron Corp., Canton, MA) [23]. The test was conducted in air at a relative humidity of about 50% to measure the flexural strength and elastic modulus. Fracture toughness was measured by using a single-edge-V-notched beam method that has been extensively studied in a round robin commissioned by the VAMAS and is currently an ISO draft [30]. A notch of a depth of approximately 800 μm was machined into the 3 mm wide surface (4 mm depth) of each specimen using a diamond blade of a thickness of 150 μm [31]. Diamond paste of 3 μm was then placed into the notch tip, and a sharp razor blade was used to further cut the notch to a total depth of about 1 mm [30, 31]. Five specimens were cut simultaneously by mounting bars side by side, sandwiched between two bars of the same material (dummy bars). The purpose of using the dummy bars was to avoid chipping at groove entry and exit points, and to aid in maintaining an even notch depth [30]. A new blade was used for each specimen group. This method was shown to produce a notch tip diameter of 20 μm or less [31]. Such a sharpness of the notch was deemed sufficient for a more accurate measurement of the fracture toughness compared to specimens with blunt notches [30]. For each specimen, the notch length was measured on both sides and averaged. The specimen dimensions were measured, and the notched specimen was fractured in three-point flexure with the notch on the tensile side, the loading pin aligned with the notch, at a span of 20 mm, and a crosshead speed of 1 mm/min. The fracture toughness

was then calculated using the single-edged-notched beam equations [30, 31].

2c. Density and porosity

The halves of specimens from the flexural test from which the mannitol was dissolved were used to measure the density and porosity. The ends of each specimen were polished with 600 SiC paper to render them flat and approximately parallel [23]. The specimens were dried in a vacuum oven (Model DP-21, American Scientific Products, McGaw Park, IL) at 60 °C for 24 h. As described in a previous study [23], the density, d, of the material was measured by using the specimen mass divided by the specimen volume. The volume was calculated from the specimen dimensions, measured with a micrometer, with each linear dimension the average of three locations along the specimen. A previous study showed that this method yielded density values that closely matched those measured by a mercury intrusion method [23].

The porosity of the specimen, P, can be obtained by

$$P = (d_{HA+CN} - d)/d_{HA+CN} \quad (1)$$

where d_{HA+CN} in the present study is the density of the fully-dense hydroxyapatite composite containing 15% chitosan, and the subscript "HA + CN" represents the hydroxyapatite + chitosan composite. The density of fully-dense hydroxyapatite without chitosan, $d_{HA,}$ is 3.14 g/cm^3 [22, 23], and d is the measured density of the specimen. In order to calculate P, d_{HA+CN} needs to be known. d_{HA+CN} can be estimated from the following.

In a theoretical fully-dense hydroxyapatite composite containing chitosan, the total specimen volume is $V = V_{HA} + V_{CN}$, and the total mass is $W = W_{HA} + W_{CN}$, where the subscript "CN" stands for chitosan. Hence

$$d_{HA+CN} = W/V = (d_{HA} + d_{CN}V_{CN}/V_{HA})/(1 + V_{CN}/V_{HA}) \quad (2)$$

In the present study, it took 0.67 g of paste to yield a specimen of approximately 3 mm × 4 mm × 25 mm, in which there was 0.023 g of chitosan. Since the density of chitosan lactate is 0.55 g/cm^3 [32], the volume of chitosan in the specimen is 0.042 cm^3. Hence Equation (2) yields $d_{HA+CN} = 2.82$ g/cm^3 for the hydroxyapatite-chitosan composite. This allows P to be calculated by using Equation (1) and the measured d for each specimen.

2d. X-ray diffraction, microscopy and statistics

Hydroxyapatite formation was examined with X-ray diffraction (XRD) [33, 29]. The 002 peak intensity of hydroxyapatite was used to measure the percentage of conversion to hydroxyapatite for the CPC−chitosan specimens. The specimens were immersed in the physiological solution for three days to leach out the mannitol crystals before the XRD of hydroxyapatite was performed. The specimens were then milled into powder by mortar and pestle, and the XRD patterns were recorded with a powder X-ray diffractometer (Rigaku, Danvers, MA) using graphite-monochromatized copper K_α radiation ($\lambda = 0.154$ nm) generated at 40 kV and 40 mA. All data were collected in a continuous scan mode ($1^\circ\ 2\theta$ min^{-1}, step time 0.6 s, step size 0.01 °) and stored in a computer.

Selected specimen surfaces were examined with a scanning electron microscope (SEM, model JSM-5300, JEOL, Peabody, MA). One standard deviation is given as the estimated standard uncertainty of the measurements. Two-way and one-way ANOVA were performed to detect significant effects. Tukey's multiple comparison was used to compare the data at a family confidence coefficient of 0.95. These results should not be compared with data obtained in other laboratories under different conditions.

3. Results

SEM micrographs of specimen surfaces are shown in Fig. 1: (A) CPC-chitosan control with 0% mannitol (no macropores); (B) CPC-chitosan composite with 45% mass fraction of mannitol; and (C) CPC-chitosan composite with 75% mannitol. The macropores from mannitol dissolution appeared to be well-formed in the shapes of the entrapped mannitol crystals. Examination of several areas of the specimens indicated that the size of macropores ranged from about 50 μm to 200 μm. There was no noticeable difference in macropore size or shape between specimens of different mannitol mass fractions. Higher magnification, Fig. 2A, shows a macropore that is nearly rounded. Figure 2B shows a macropore that is highly elongated (long arrow), together with an irregularly shaped macropore that is probably produced by the dissolution of several mannitol particles in contact (short arrows). In Fig. 2C, the arrow indicates open connections between macropores.

CPC conversion to hydroxyapatite is plotted in Fig. 3 as a function of mannitol mass fraction. Error bars show one standard deviation. The mannitol particles were dissolved during immersion to create macropores in CPC-chitosan composite prior to XRD analysis. The percentage (%) of CPC converted to hydroxyapatite increased from 75.3 % for CPC-chitosan composite containing 0% mannitol, to 85.7 % for composite containing 15 % mannitol, and to 99.8 % for composite containing 60 % mannitol. The conversion then plateaued, with the conversion at 75 % mannitol being 97.8 %, not significantly different from the conversion for the composite with 60% mannitol ($p > 0.1$).

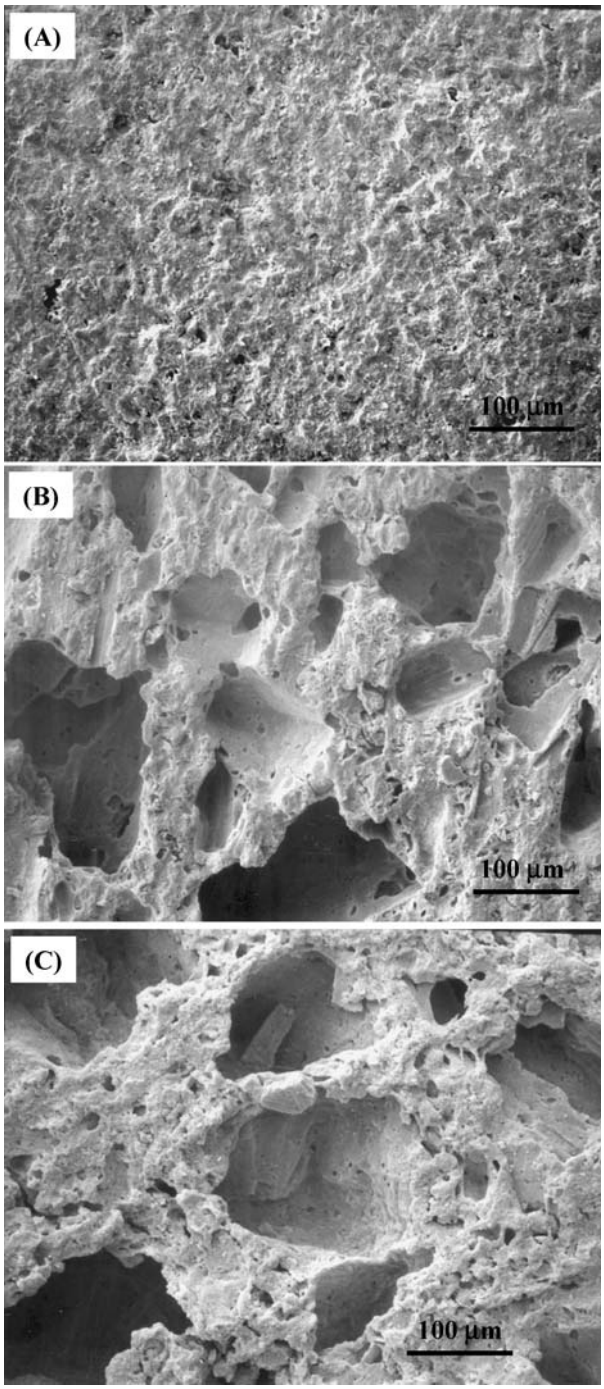

Fig. 1 SEM micrographs: (A) CPC-chitosan with 0% mannitol showing no macropores; (B) CPC-chitosan composite with 45% mass fraction of mannitol; and (C) CPC-chitosan composite with 75% mannitol. The macropores in (B-C) appeared to be well-formed in the shapes of the entrapped mannitol crystals.

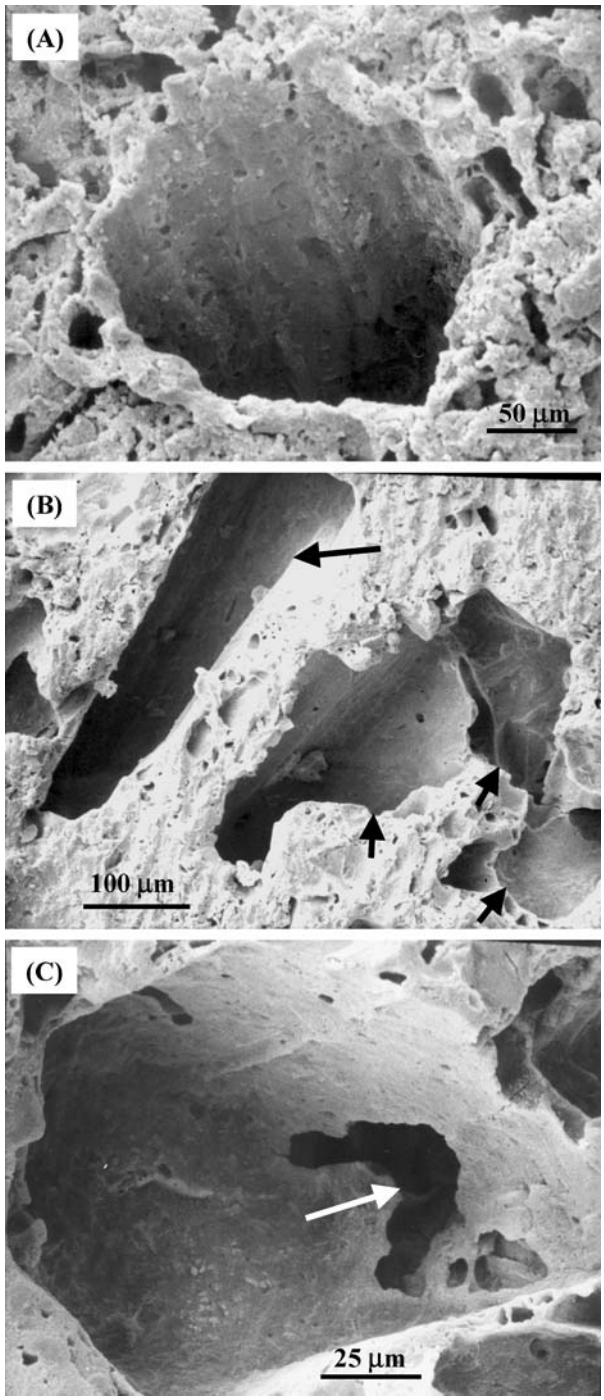

Fig. 2 (A) nearly round-shaped macropore in CPC with 75% mannitol; (B) elongated macropore (long arrow) in CPC with 45% mannitol, and an irregularly-shaped macropore that was likely a result of dissolution of several mannitol particles (short arrows); and (C) open connection in the wall of a macropore in CPC with 45% mannitol (arrow).

Specimen density and porosity are shown in Fig. 4 as a function of mannitol mass fraction. Each value was the mean of six measurements with the error bar showing one standard deviation. Density (mean $\pm$ sd; n = 6) was measured to be (1.85 ± 0.03) g/cm^3 at 0% mannitol. It decreased to (0.84 ± 0.01) g/cm^3 at 45% mannitol, and (0.47 ± 0.01) g/cm^3 at 75% mannitol. Meanwhile, the pore volume fraction in the specimens increased from 34.4% at 0% mannitol, to 70.2% at 45% mannitol, and further to 83.3% for the scaffold that contained 75% mannitol.

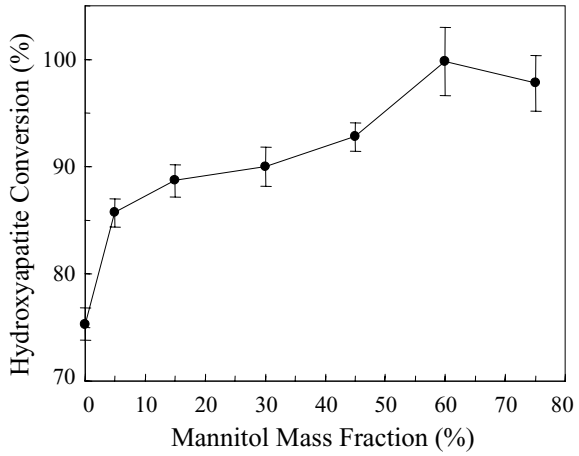

Fig. 3 XRD analysis of the percentage (%) of CPC converted to hydroxyapatite as a function of mannitol mass fraction at 3 d. Error bars show one standard deviation (sd), and the line connects the data points.

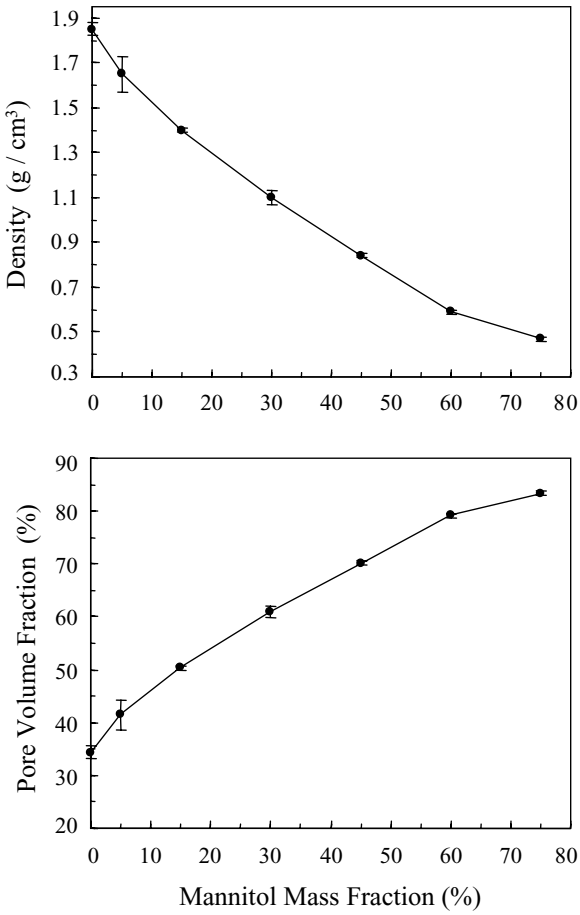

Fig. 4 Density and porosity of CPC-chitosan scaffold after mannitol dissolution to create macropores as a function of mannitol mass fraction. Each value was the mean of six measurements with the error bar showing one standard deviation. The line connects the data points.

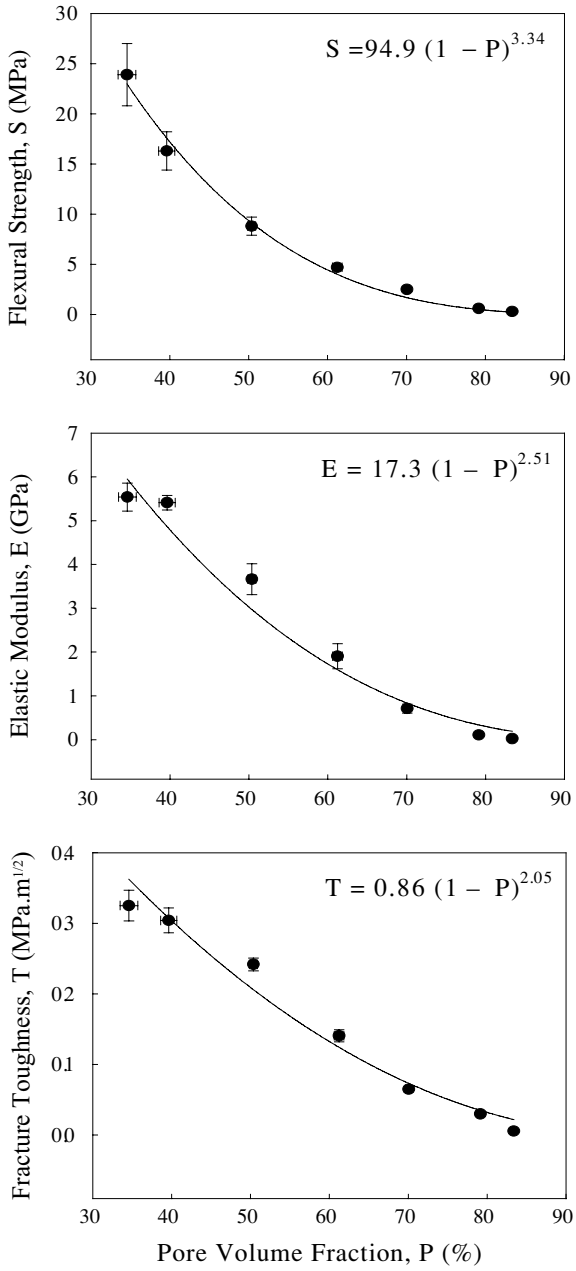

Fig. 5 Flexural strength, elastic modulus and fracture toughness vs. porosity for the *in situ* hardening CPC-chitosan scaffold. Each value is the mean of six measurements with the error bar showing one standard deviation. Note that the origin "0" of the y-axis is away from the x-axis for clarity. The solid lines are power-law regression fits of Equations (6–8) to the measured data, resulting in the establishment of Equations (9–11).

Figure 5 plots flexural strength, elastic modulus, and fracture toughness as functions of pore volume fraction after the mannitol crystals were dissolved to create macropores. The data are the measured values with the error bars showing one standard deviation. Flexural strength, elastic modulus, and fracture toughness decreased precipitously with increasing the pore volume fraction. The strength at 34.4% porosity

(mean ± sd; n = 6) was (23.9 ± 3.1) MPa; it decreased by nearly two orders of magnitude to (0.3 ± 0.1) MPa at 83.3% porosity. Similar decreases occurred for elastic modulus and fracture toughness. The solid curves in Fig. 5 are regression power-law fits to the measured data. The equations in Fig. 5 show relationships between mechanical properties and porosity, and will be described in the Discussion section.

4. Discussion

Conventional CPC has been described as having three major short-comings: relatively low strength; long setting time accompanied by washout prior to setting; and slow resorption and replacement by new bone. Low strength and high susceptibility to brittle fracture limited the use of CPC to non load-bearing applications [17–21]. Unset cement washout can occur *in vivo* in physiological fluids or when bleeding occurs due to incomplete hemostasis [34]. Macroporosity could be beneficial in CPC because macropores have been shown to facilitate cell infiltration and tissue ingrowth [1–5]. Recently, efforts were undertaken to overcome these three short-comings.

Chitosan and its derivatives are natural biopolymers that are biocompatible, biodegradable and osteoconductive [24–26]. Chitosan lactate had been incorporated into CPC [27, 28]. While earlier versions of CPC paste took > 60 min to harden, CPC-chitosan lactate pastes hardened in 6.7 min [27, 28]. Fast-setting was accompanied by an anti-washout characteristic, manifested by a lack of dissolution of freshly-mixed CPC-chitosan paste when immersed in a physiological solution. In comparison, the conventional CPC paste without chitosan showed significant dissolution and washout in the same solution [27, 28]. The hardening mechanism for the conventional CPC was the reaction between TTCP and DCPA leading to the formation of hydroxyapatite. TTCP ($Ca_4(PO_4)_2O$) and DCPA ($CaHPO_4$) dissolved in water as Ca^{2+}, PO_4^{3-} and OH^- ions, which then reprecipitated to form hydroxyapatite, $Ca_{10}(PO_4)_6(OH)_2$. In contrast, for CPC containing chitosan, another faster reaction occurred besides the usual TTCP-DCPA reaction, resulting in faster-setting. Chitosan and its derivatives are soluble in acidic solutions, but insoluble in solutions with neutral or alkaline pH. The mixing of the CPC powder with the chitosan liquid increased the pH to above 7, causing the soft CPC-chitosan paste to transform to a hard mass. The initial hardening of the CPC paste containing chitosan was caused not by the TTCP-DCPA conversion to hydroxyapatite, which was slower, but by the chitosan hardening due to a pH increase, which was faster. The increased viscosity of the cement paste due to the addition of chitosan which served as a gelling agent, together with its fast setting, appeared to have contributed to the washout resistance of the cement paste when immersed in a physiological solution [28]. Furthermore, the addition of chitosan has also been shown to increase the graft strength and work-of-fracture significantly [29].

In the present study, a wide range of porosity was created in the CPC-chitosan composite with pore volume fraction up to 83.3%. The macropores were created by using a readily-soluble porogen (mannitol) because it has the appropriate solubility, is non-toxic, and is physiologically compatible [22, 23]. Currently-available sintered hydroxyapatite implants required machining, hence achieving a good fit into a complex bone cavity could be difficult. In contrast, the present CPC-mannitol powder could be mixed with the chitosan-water liquid into a formable paste that could conform to bone defects. The paste could also be applied via minimally invasive techniques such as injection [16], with fast-setting and anti-washout capabilities [27, 28] to form a highly porous hydroxyapatite scaffold *in situ*.

The flexural strength of sintered porous hydroxyapatite implants ranged from 2 MPa to 11 MPa [5], whereas cancellous bone has a reported tensile strength of about 3.5 MPa [35]. These strength values were similar to those at mannitol fractions of 30% and 45%, which yielded a porosity of 60 % to 70 %. The elastic modulus of cancellous bone ranged from 50 MPa to 300 MPa [36]. The scaffold with 70 % to 79 % porosity had a comparable range of elastic modulus from 110 MPa to 710 MPa. It should be noted that the strength and elastic modulus of bone depend on the type and location of bone, for example, craniofacial bone versus long bone. Hence the mimicking of natural bone properties in the development of bone substitutes needs to be bone type-specific.

The mannitol particles used here to create macropores in CPC had a diameter of (165 ± 44) μm and a length of (271 ± 72) μm [28]. The macropore sizes of the scaffolds ranged from about 50 μm to 200 μm (Fig. 4), somewhat smaller than the starting mannitol particle size. This is probably because some of the surface of the mannitol particles was dissolved during the mixing of the CPC paste. Nonetheless, pore diameters ranging from 50 μm to 200 μm should be useful for cell infiltration and bone ingrowth, as shown in earlier studies [37–41]. A previous study showed that osteoblast cell sizes including the cytoplasmic extensions ranged from about 20 μm to 60 μm [42]. Regarding pore volume fraction, previous studies on sintered hydroxyapatite implants showed porosities from about 40 % to 48 % and as high as 75 % [38, 39]. These values were consistent with the scaffold porosity range of the present study. In addition, because CPC could be bio-resorbed, the pore sizes and pore volume fractions of the CPC scaffold would increase over time *in vivo*.

The percentage of CPC conversion to hydroxyapatite first increased with mannitol mass fraction from 0 % to 60 %,

and then plateaued when the mannitol fraction was further increased from 60 % to 75 % (Fig. 3). With mannitol dissolution and macropore formation, the surface area of the scaffold was increasing with higher mannitol fraction. This improved the contact of the physiological solution with the TTCP and DCPA particles in the scaffold, and likely enhanced their reaction and hence the CPC conversion to hydroxyapatite. The plateau at higher mannitol fractions was due to the CPC achieving nearly full conversion to hydroxyapatite. The CPC-chitosan composite with 0 % mannitol had a conversion of 75.3 %, slightly lower than a conversion of 80.3 % measured in a previous study for CPC containing the same chitosan mass fraction of 15 % [29]. This small difference in hydroxyapatite conversion may be because the powder:liquid ratio of 1 used in the previous study was lower than the 3.5 ratio in the present study, and the extra liquid in the paste may have facilitated the CPC conversion to hydroxyapatite.

The effects of porosity on mechanical properties of hydroxyapatite [43–45] and calcium phosphate cements [11, 46] have been investigated in previous studies. Several studies [11, 43, 45, 46] have used an empirical relationship between strength, S, and porosity, P:

$$S = S_0 e^{-bP} \tag{3}$$

where S_0 is the theoretical strength at $P = 0$ (fully-dense), and b is an empirical constant.

Other studies have modeled porous ceramics as an elastic-brittle foam and yield the following relationship [44, 47]:

$$S = \alpha d^x \tag{4}$$

$$E = \beta d^y \tag{5}$$

where d is the density of the specimen, and α, β, x and y are constants. Equations (4, 5) were used in the present study to describe the porosity-mechanical property relationships, because they predict that when the density $d = 0$, $S = 0$ and $E = 0$.

From Equation (1), $d = d_{HA+CN}(1 - P)$. Inserting this into Equations (4, 5) yields

$$S = S_0(1 - P)^x \tag{6}$$

$$E = E_0(1 - P)^y \tag{7}$$

Equation (6) shows that when porosity $P = 1$, $S = 0$. When $P = 0$ (fully-dense), $S = S_0$, which is the strength for fully-dense specimens. The same is true for E in Equation (7). Assuming that the same relationship also holds for fracture toughness, T:

$$T = T_0(1 - P)^z \tag{8}$$

where z is a constant, and T_0 is toughness for fully-dense specimens.

By fitting Equations (6–8) to the measured properties, the best fits were obtained and are shown in Fig. 5. The solid lines in Fig. 5 are regression power-law fits to the measured data, with $R^2 = 0.99$, 0.98, 0.99, for strength, elastic modulus and fracture toughness, respectively. The regression coefficients for Equations 5–7 resulted in the following relationships:

$$S = 94.9(1 - P)^{3.34}\ \text{MPa} \tag{9}$$

$$E = 17.3(1 - P)^{2.51}\ \text{GPa} \tag{10}$$

$$T = 0.86(1 - P)^{2.05}\ \text{MPa} \cdot \text{m}^{1/2} \tag{11}$$

The fitting yielded $S_0 = 94.9$ MPa for flexural strength of fully-dense specimens, which is within the reported bending strength range of 38 MPa to 250 MPa for dense hydroxyapatite [5]. E_0 of 17.3 GPa is lower than the reported elastic modulus of 35 GPa to 120 GPa for dense hydroxyapatite [5]. This is likely because the composite of the present study contained chitosan, which was shown to be a relatively non-rigid material with a low elastic modulus [29]. For fracture toughness, the fitting yielded $T_0 = 0.86$ MPa·m$^{1/2}$ for fully-dense specimens, consistent with the reported range of 0.8 MPa·m$^{1/2}$ to 1.2 MPa·m$^{1/2}$ for dense hydroxyapatite [5]. While the general relationships in Equations (6–8) may be applicable to other scaffold systems, the actual coefficients may be material-specific and will need to be individually determined to establish predictive models such as Equations (9–11).

5. Summary

CPC-chitosan scaffolds were investigated with porosities up to 83.3%. Flexural strength, elastic modulus and fracture toughness were determined as functions of mannitol mass fraction and pore volume fraction. The new scaffold approximated the strength and elastic modulus of sintered porous hydroxyapatite implants and cancellous bone. Relationships between porosity and mechanical properties were determined, describing the dependence of flexural strength, elastic modulus, and fracture toughness on scaffold porosity. The new graft composition could be delivered during surgery in the form of a paste to harden *in situ* into macroporous hydroxyapatite. Compared to the conventional CPC without macropores, the increased macroporosity of the new apatite scaffold may help facilitate bone ingrowth, implant fixation, and more rapid new bone formation.

Acknowledgements We thank Drs. B. R. Lawn, F. C. Eichmiller and S. H. Dickens for discussions, and A. A. Giuseppetti for experimental assistance. This study was supported by USPHS grants DE14190 (Xu) and DE11789 (Chow), NIST, and the ADAF.

Disclaimer

Certain commercial materials and equipment are identified in this paper to specify experimental procedures. In no instance does such identification imply recommendation by NIST or the ADA Foundation or that the material identified is necessarily the best available for the purpose.

References

1. C. T. LAURENCIN, A. M. A. AMBROSIO, M. D. BORDEN and J. A. COOPER Jr., *Annu. Rev. Biomed. Eng.* **1** (1999) 19.
2. R. LANGER and J. VACANTI, *Science* **260** (1993) 920.
3. L. L. HENCH and J. WILSON, An Introduction to Bioceramics (World Scientific, New Jersey, 1993).
4. K. A. HING, S. M. BEST, K. E. TANNER, W. BONFIELD and P. A. REVELL, *J. Biomed. Mater. Res.* **68A** (2004) 187.
5. W. SUCHANEK and M. YOSHIMURA, *J. Mater. Res.* **13** (1998) 94.
6. W. E. BROWN and L. C. CHOW, p. 352 in Cements Research Progress, P. W. Brown, editor, (American Ceramic Society, OH, USA, 1986).
7. M. P. GINEBRA, E. FERNANDEZ, E. A. P. DE MAEYER, R. M. H. VERBEECK, M. G. BOLTONG, J. GINEBRA, F. C. M. DRIESSENS and J. A. PLANELL, *J. Dent. Res.* **76** (1997) 905.
8. B. R. CONSTANTZ, B. M. BARR, I. C. ISON, M. T. FULMER, J. BAKER, L. MCKINNEY, S. B. GOODMAN, S. GUNASEKAREN, D. C. DELANEY, J. ROSS and R. D. POSER, *J. Biomed. Mater. Res. (Appl. Biomater.)* **43** (1998) 451.
9. D. KNAACK, M. E. P. GOAD, M. AIOLOVA, C. REY, A. TOFIGHI, P. CHAKRAVARTHY and D. D. LEE, *J. Biomed. Mater. Res. (Appl. Biomater.)* **43** (1998) 399.
10. Y. MIYAMOTO, K. ISHIKAWA, M. TAKECHI, T. TOH, T. YUASA, M. NAGAYAMA and K. SUZUKI, *J. Biomed. Mater. Res. (Appl. Biomater.)* **48** (1999) 36.
11. J. E. BARRALET, T. GAUNT, A. J. WRIGHT, I. R. GIBSON and J. C. KNOWLES, *J. Biomed. Mater. Res. (Appl. Biomater.)* **63** (2002) 1.
12. A. YOKOYAMA, S. YAMAMOTO, T. KAWASAKI, T. KOHGO and M. NAKASU, *Biomaterials* **23** (2002) 1091.
13. A. GISEP, R. WIELING, M. BOHNER, S. MATTER, E. SCHNEIDER and B. RAHN, *J. Biomed. Mater. Res.* **66** (2003) 532.
14. A. EHARA, K. OGATA, S. IMAZATO, S. EBISU, T. NAKANO and Y. UMAKOSHI, *Biomaterials* **24** (2003) 831.
15. T. YUASA, Y. MIYAMOTO, K. ISHIKAWA, M. TAKECHI, Y. MOMOTA, S. TATEHARA and M. NAGAYAMA, *Biomaterials*, **25** (2004) 1159.
16. D. APELT, F. THEISS, A. O. EL-WARRAK, K. ZLINSZKY, R. BETTSCHART-WOLFISBERGER, M. BOHNER, S. MATTER, J. A. AUER and B. VON RECHENBERG, *Biomaterials*, **25** (2004) 1439.
17. C. D. FRIEDMAN, P. D. COSTANTINO, K. JONES, L. C. CHOW, H. J. PELZER and G. A. SISSON, *Arch. Otolaryngol. Head Neck Surg.* **117** (1991) 385.
18. P. D. COSTANTINO, C. D. FRIEDMAN, K. JONES, L. C. CHOW and G. A. SISSON, *Plast. Reconstr. Surg.* **90** (1992) 174.
19. M. L. SHINDO, P. D. CONTANTINO, C. D. FRIEDMAN and L. C. CHOW, *Arch. Otolaryngol. Head Neck Surg.* **119** (1993) 185.
20. C. D. FRIEDMAN, P. D. COSTANTINO, S. TAKAGI and L. C. CHOW, *J. Biomed. Mater. Res. (Appl. Biomater.)* **43** (1998) 428.
21. L. C. CHOW, *Mat. Res. Symp. Proc.* **599** (2000) 27.
22. S. TAKAGI and L. C. CHOW, *J. Mater. Sci.: Mater. Med.* **12** (2001) 135.
23. H. H. K. XU, J. B. QUINN, S. TAKAGI, L. C. CHOW and F. C. EICHMILLER, *J. Biomed. Mater. Res.* **57** (2001) 457.
24. Y. MACHIDA, T. NAGAI, M. ABE and T. SANNAN, *Drug. Dis. Deliv.* **1** (1986) 119.
25. R. A. A. MUZZARELLI, G. BIAGINI, M. BELLARDINI, L. SIMONELLI, C. CASTALDINI and G. FRAATTO, *Biomaterials* **14** (1993) 39.
26. R. A. A. MUZZARELLI, P. 87 IN CHITIN and CHITOSAN and G. SKJAK-BRAK, T. ANTHONSEN, P. SANDFORD, editors, (Elsevier Applied Sci., NY, 1989).
27. S. TAKAGI, L. C. CHOW, S. HIRAYAMA and F. C. EICHMILLER, *Dent. Mater.* **19** (2003) 797.
28. H. H. K. XU, S. TAKAGI, J. B. QUINN and L. C. CHOW, *J. Biomed. Mater. Res.* **68**A (2004) 725.
29. H. H. K. XU, J. B. QUINN, S. TAKAGI and L. C. CHOW, *J. Dent. Res.* **81** (2002) 219.
30. The Versailles Project on Advanced Materials and Standards (VAMAS) and The European Structural Integrity Society (ESIS). Fracture toughness of ceramics using the SEVNB method; round robin. Swiss Federal Laboratories for Materials Testing and Research (1999).
31. H. H. K. XU, J. B. QUINN and A. A. GIUSEPPETTI, *J. Dent. Res.* **83** (2004) 930.
32. Materials Safety Data Sheet, Rita Corp., Woodstock, IL, USA, updated 2003.
33. Y. FUKASE, E. D. EANES, S. TAKAGI, L. C. CHOW and W. E. BROWN, *J. Dent. Res.* **69** (1990) 1852.
34. K. ISHIKAWA, Y. MIYAMOTO, M. TAKECHI, T. TOH, M. KON, M. NAGAYAMA and K. ASAOKA, *J. Biomed. Mater. Res.* **36** (1997) 393.
35. C. J. DAMIEN and J. R. PARSONS, *J. Appl. Biomater.* **2** (1991) 187.
36. K. O'KELLY, D. TANCRED, B. MCCORMACK and A. CARR, *J. Mater. Sci.: Mater. Med.* **7** (1996) 207.
37. E. C. SHORS and R. E. HOLMES, P. 181 IN L. L. HENCH and J. WILSON, editors, An introduction to bioceramics (World Scientific, New Jersey, 1993).
38. R. M. PILLIAR, M. J. FILIAGGI, J. D. WELLS, M. D. GRYNPAS and R. A. KANDEL, *Biomaterials*, **22** (2001) 963.
39. N. TAMAI, A. MYOUI, T. TOMITA, T. NAKASE, J. TANAKA, T. OCHI and H. YOSHIKAWA, *J. Biomed. Mater. Res.* **59** (2002) 110.
40. E. TSURUGA, H. TAKITA, H. ITOH, Y. WAKISAKA and Y. KUBOKI, *J. Biochem.* **121** (1997) 317.

41. E. DAMIEN, K. HING, S. SAEED and P. A. REVELL, *J. Biomed. Mater. Res.* **66** (2003) 241.
42. H. H. K. XU and C. G. SIMON, *J. Orthopedic Res.* **22** (2004) 535.
43. D. M. LIU, *Ceram. Intl.* **23** (1997) 135.
44. K. A. HING, S. M. BEST and W. BONFIELD, *J. Mater. Sci.: Mater. Med.* **10** (1999) 135.
45. L. M. RODRÍGUEZ-LORENZO, M. VALLET-REGÍ, J. M. F. FERREIRA, M. P. GINEBRA, C. APARICIO and J. A. PLANELL, *J. Biomed. Mater. Res.* **60** (2002) 159.
46. K. ISHIKAWA and K. ASAOKA, *J. Biomed. Mater. Res.* **29** (1995) 1537.
47. L. J. GIBSON, *J. Biomech.* **18** (1985) 317.